NASA TECHNICAL NOTE

NASA TN D-2904

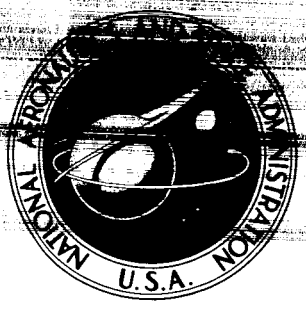

NASA TN D-2904

DIRECTIONAL THERMAL-RADIATIVE PROPERTIES OF CONICAL CAVITIES

by Leslie G. Polgar and John R. Howell

Lewis Research Center

Cleveland, Ohio

NATIONAL AERONAUTICS AND SPACE ADMINISTRATION • WASHINGTON, D. C. • JUNE 1965

NASA TN D-2904

DIRECTIONAL THERMAL-RADIATIVE PROPERTIES OF CONICAL CAVITIES

By Leslie G. Polgar and John R. Howell

Lewis Research Center
Cleveland, Ohio

NATIONAL AERONAUTICS AND SPACE ADMINISTRATION

For sale by the Clearinghouse for Federal Scientific and Technical Information
Springfield, Virginia 22151 – Price $2.00

DIRECTIONAL THERMAL-RADIATIVE PROPERTIES OF CONICAL CAVITIES

by Leslie G. Polgar and John R. Howell

Lewis Research Center

27273

SUMMARY

27273

A Monte Carlo technique is applied to the problem of finding the apparent directional thermal-radiative reflectance, absorptance, and emittance of a right circular conical cavity with a diffusely reflecting internal surface. Parameters examined are the cone angle, the cone surface absorptivity, and the angle of incident radiation. Small cone angles are found to produce a strong reflection back to the direction of incident radiation, while the results for large cone angles approach those for a flat plate. The Monte Carlo method is found to give a useful tool for solving problems of this type. The directional emittance results may be useful in the field of optical pyrometry, where the effect of viewing angle on the apparent temperature of a cavity is of interest. Some correlation to the reflection properties of the Moon are noted.

Author

INTRODUCTION

The directional radiative properties of surfaces are nearly always neglected when calculations involving radiative-energy transfer are made. This is due both to the lack of experimental data on directional effects for real surfaces and to the difficulty of including such data in routine calculations. The reflection laws usually assumed are for diffuse (cosine law) or specular (mirrorlike) reflections, or some combination of these, as suggested in reference 1. The former mode assumes the reflections to be independent of the angle of incident radiation, while the latter assumes the simplest possible relation between angle of incidence and reflection, that is, the angle of incidence equal to minus the angle of reflection. Both cause a great reduction in the complexity of calculation.

Most common surfaces do not reflect in either a specular or a diffuse manner. The Moon is one common example (ref. 2) where the reflectance[1] of visible radiation is

---

[1]In this report, the ending "ance" (i.e., reflectance) refers to apparent surface properties, whereas the "ivity" ending (reflectivity) refers to a physical property of the material.

strongest back in the direction of the incident radiation. More discussion of this is given in the DISCUSSION OF RESULTS. It has also been shown (refs. 3 and 4) that cavities of various shapes can greatly alter the directional reflective and emissive properties of surfaces and can reflect energy back in the direction of incident radiation.

Two-dimensional shapes can be analyzed by standard methods involving formulation of the energy exchange equations in terms of "shape" or "exchange" factors available in the literature for many simple geometries. Some shape factors for three-dimensional bodies can be found in the literature, but the complexity of formulation of radiative exchange problems becomes great. For example, Sparrow and Jonsson (ref. 5) treated the relatively simple case of finding the total hemispherical emittance of a conical cavity assumed to be either at constant surface temperature or having uniform surface energy flux.

In this report, a Monte Carlo method is used as an alternate approach to the usual shape factor formulation in finding the directional properties of a conical cavity, with a view to developing some insight into surface anomalies and developing a useful technique for solving problems of this type. The results are useful in determining the accuracy of pyrometrical measurements of the surface temperature when this temperature is measured by viewing a cavity in the surface.

SYMBOLS

A	area of element on hemisphere over reflecting surface
B	$\cos \zeta' / \cos \theta$
C	$\cos \zeta' \sin \eta' \cos \psi' / \cos \theta$
G	$\cot \theta / \cot \zeta$
ℓ	path length of bundle between reflections
P	probability of incident energy bundle striking given illuminated area element on internal surface of cone
R	number chosen at random from evenly distributed set of numbers in range 0 to 1
r	distance along element of cone
X, Y, Z	Cartesian coordinate system defined in fig. 7(a), Z being on or parallel to the cone axis and X being the line of intersection of the cone base and the plane perpendicular to the base and parallel to the incident radiation
X', Y', Z'	coordinate system defined in figs. 2 and 7(a)

α_a apparent absorptance of cavity

α_s surface absorptivity

γ angle between lines in base plane parallel to projections of bundle path and incident energy, fig. 1

δ incremental value

ζ angle between cone axis and line through cone axis parallel to incident radiation, angle of incidence

η angle between normal to cone wall at point of bundle path intersection and bundle path

θ cone half-angle

μ local cone radius at point of bundle reflection

ρ directional reflectance of conical cavity

φ circumferential angle around cone axis, measured counterclockwise from X-axis to μ

ψ angle from X'-axis to projection of bundle path in plane tangent to cone wall at point of bundle intersection

Ω variable

Subscripts:

i, j angular increment indices

max maximum

min minimum

p projected normal to direction of incident radiation

ζ, ζ', γ' function of directions ζ, ζ', and γ', respectively

Superscript:

' values after reflection

ANALYSIS

Incident parallel radiation, assumed to consist of discrete bundles of energy, is impinging at a given angle on a right circular conical cavity of known surface absorptivity. The base radius of the cone is used to nondimensionalize all lengths in the analysis. The walls of the cone are assumed to be gray and diffusely reflecting; polarization effects

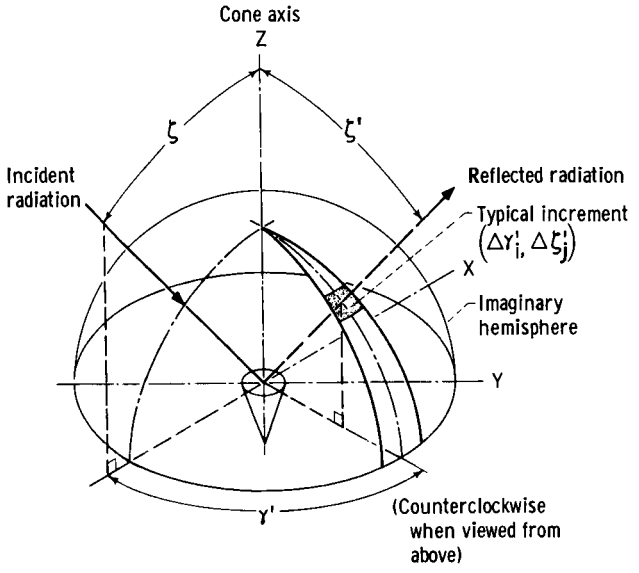

Figure 1. - Coordinates for energy bundles reflected from conical cavity.

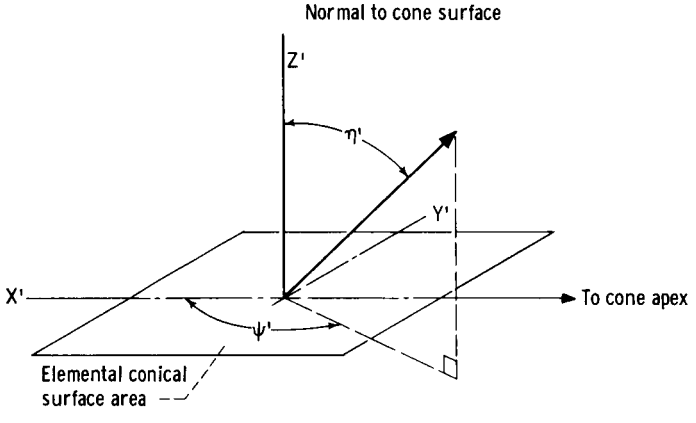

Figure 2. - Angles of reflection from conical surface.

are not considered. It is assumed that no energy is emitted from the cone walls (i. e., the cone is cold compared to the source of incident radiation).

A Monte Carlo method is used to find the apparent absorptance and the distribution of reflected energy from the conical cavity. This method consists of following each discrete bundle of incident energy through its probable path in the region of the cone, taking into account the diffuse reflections within the cone and the absorption of energy bundles at the gray internal surface. Those bundles which leave the cone are tallied in the angular increment $\Delta\gamma'_i, \Delta\zeta'_j$ on an imaginary hemisphere over the mouth of the cone (fig. 1) from which they leave.

The initial point (μ, φ) where the bundle strikes and the question of whether or not the bundle is absorbed or reflected at that point are both determined by a Monte Carlo technique. If it is absorbed, this is tallied. If it is reflected, the direction of reflection is specified by two angles, ψ' and η' (fig. 2), that are chosen at random from the properly weighted set of angles of reflection. It is determined whether the reflected bundle exits from the cone or traverses the cavity and intersects the cone wall at another point. Exiting bundles are classified by their angular coordinates (γ' and ζ'). Bundles that strike the cone wall a second time are again checked to see if absorption occurs at this point. The internal reflection process is continued until the bundle is either absorbed or leaves the cavity.

The apparent absorptance $\alpha_{a,\zeta}$, defined here as the fraction of energy incident from a given direction ζ that is absorbed within the conical cavity, is then simply the fraction of incident bundles that is absorbed within the cavity. Defining the directional reflectance $\rho_{\zeta,\zeta',\gamma'}$ as the fraction of energy incident from direction ζ that is reflected per unit solid angle around ζ', γ' allows determination of this value by tallying

the fraction of total incident bundles that leave in each unit solid angle.

Point of Initial Bundle Intersection

The illuminated area of an element on the conical surface projected normal to the direction of incident radiation is given by

$$dA_p = \cos \eta \, dA \tag{1}$$

where the area of an element of the conical surface is given by

$$dA = \mu \csc \theta \, d\mu \, d\varphi \tag{2}$$

and $\cos \eta$ is found in terms of known quantities by projecting a unit vector of incident radiation onto the normal to the cone wall at the point of intersection. This is done directly and by components (appendix A, eq. (A7)) to give

$$\cos \eta = \sin \theta \cos \zeta + \cos \theta \sin \zeta \cos \varphi \tag{3}$$

The probability of an incident energy bundle striking a given illuminated area element on the internal surface of the cone is the projected area of that element over the total projected illuminated area:

$$P(d\mu \, d\varphi) = \frac{\cos \eta \, dA}{\int_A \cos \eta \, dA} \tag{4}$$

This probability can be separated into the probabilities of a bundle striking an element $d\mu$ and an element $d\varphi$ because substitution of equations (2) and (3) into equation (4) indicates that μ and φ appear only as products and are therefore independent in the probability sense. The separation gives

$$P(d\mu) = \int_{\varphi_{min}}^{\varphi_{max}} P(d\mu \, d\varphi) \tag{5}$$

and

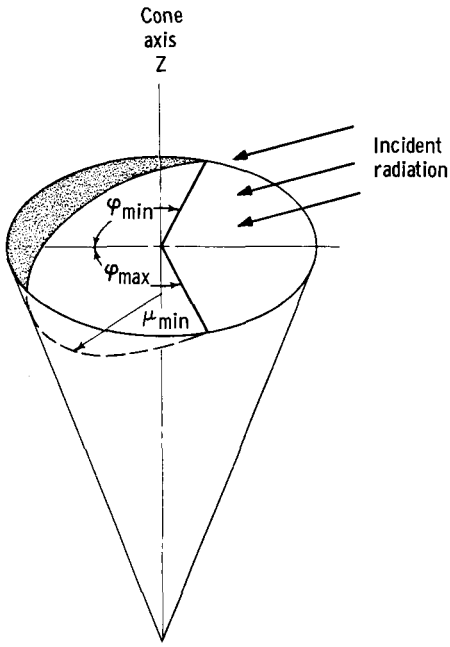

Figure 3. - Graphic definitions of μ_{min}, φ_{min}, and φ_{max}. The boundary of the area visible to the incident radiation is defined by μ_{min} which is the least μ defined for a given φ, where $\varphi_{min} \leq \varphi \leq 0$ or $0 \leq \varphi \leq \varphi_{max}$.

$$P(d\varphi) = \int_{\mu_{min}}^{1} P(d\mu\ d\varphi) \tag{6}$$

When the angle of incident energy is less than the cone half-angle, that is, when $\zeta \leq \theta$, the entire inner surface is illuminated. Consequently, the local radius μ_{min} at the minimum illuminated point for any value of φ is

$$\mu_{min} = 0 \tag{7}$$

and the minimum and maximum circumferential angles φ_{max} and φ_{min} at which illumination occurs are

$$\varphi_{max} = -\varphi_{min} = \pi \tag{8}$$

For $\zeta > \theta$, part of the conical cavity is shadowed by the lip of the cone (fig. 3). For these cases, μ_{min} and φ_{max} must be calculated. From the relation

$$\left(1 - \mu_{min}^2 \sin^2\varphi\right)^{1/2} + \mu_{min} \cos\varphi = \frac{(1 - \mu_{min})\cot\theta}{\tan(90 - \zeta)} \tag{9}$$

derived from relations for the depth at which the incident radiation strikes the wall at a given φ, and for a given angle of incidence (appendix A, eq. (A11)) μ_{min} is given by

$$\mu_{min} = \frac{G(G + \cos\varphi) \mp (G\cos\varphi + 1)}{G^2 + 2G\cos\varphi + 1} \tag{10}$$

where $G = \cot\theta/\cot\zeta$. The top sign is the correct choice as examination of any special case with $\mu_{min} \neq 1$ will indicate. This choice leads to

$$\mu_{min} = \frac{G^2 - 1}{G^2 + 2G\cos\varphi + 1} \tag{11}$$

To find φ_{max} (always equal to φ_{min} by symmetry), μ_{min} is set equal to 1 in equation (11). Then

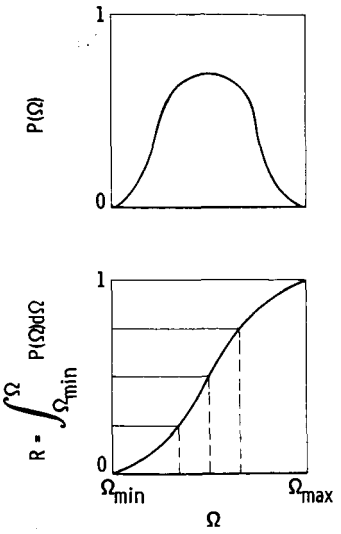

Figure 4. - Determination of distribution of Ω.

$$\cos \varphi_{max} = \frac{-1}{G} \tag{12}$$

There remains only the problem of choosing values of μ and φ such that the distributions given by equations (5) and (6), respectively, will be satisfied after enough values are chosen.

For functions that can be easily integrated, a straightforward procedure exists for doing this. The procedure consists of carrying out the integration of the probability $P(\Omega)$

$$R = \int_{\Omega_{min}}^{\Omega} P(\Omega)d\Omega \tag{13}$$

and choosing values of R in a random fashion to give values of the variable Ω. The physical meaning of this procedure is demonstrated by figure 4. Because the integral of $P(\Omega)$ over all Ω must be unity, R can only take on values in the range 0 to 1. Equation (13) gives the probability of any element $P(\Omega)d\Omega$ lying in the range Ω_{min} to Ω. Consider choosing five equally spaced values of R. If in each equal increment ΔR an equal number of values of R is chosen, for example N, the value $N/\Delta\Omega$ in each increment will be proportional to the slope in that increment. But the slope in each increment must be directly related to the probability $P(\Omega)$ corresponding to Ω for that increment since $dR/d\Omega$ at Ω is exactly $P(\Omega)$. Choosing enough values of R in small enough intervals and making sure they come from a set of R evenly distributed in the range 0 to 1 guarantee accurate derivatives. Therefore, the distribution of Ω calculated will adequately describe the original distribution $P(\Omega)$.

Equation (13) can be applied for any integrable probability distribution. For μ and φ this process gives

$$R_{\mu} = \frac{\int_{\mu_{min}}^{\mu} \mu \, d\mu}{\int_{\mu_{min}}^{\mu_{max}=1} \mu \, d\mu} \tag{14}$$

and

$$R_{\varphi} = \frac{\int_{\varphi_{min}}^{\varphi} (\cos \zeta + \cot \theta \sin \zeta \cos \varphi) d\varphi}{\int_{\varphi_{min}}^{\varphi_{max}} (\cos \zeta + \cot \theta \sin \zeta \cos \varphi) d\varphi} \tag{15}$$

respectively. Solving for μ and φ gives

$$\mu = \left[R_{\mu}\left(1 - \mu_{min}^2\right) + \mu_{min}^2\right]^{1/2} \tag{16}$$

and

$$\varphi = (2R_{\varphi} - 1)(\varphi_{max} + \cot \theta \tan \zeta \sin \varphi_{max}) - \cot \theta \tan \zeta \sin \varphi \tag{17}$$

If two numbers are chosen at random from a set of numbers evenly distributed between 0 and 1, and they are designated as R_{μ} and R_{φ}, an initial point φ at which an incident energy bundle strikes the interior surface of the cone can be chosen from equation (17). Then μ_{min} is found from equations (10) or (7) as the case may be, and μ is evaluated from equation (16).

Equation (17) is transcendental in form, involving both φ and $\sin \varphi$, and its solution requires iterative means. Because of the rapidity with which this program as a whole is expected to run, no great pains are taken to minimize running time for this step, and the Newton-Raphson technique, modified to include third-order terms, is employed (see appendix B). An iteration check is used, and if convergence is slow, an alternate regula-falsi method is used (ref. 6).

Determination of Bundle Absorption

When the original point (μ, φ) at which the bundle strikes the wall is determined, the probability of bundle absorption at that point is checked by comparing another randomly chosen number R_{α} to the surface absorptivity α_s of the cone. If

$$R_{\alpha} \leq \alpha_s \tag{18}$$

the bundle is tallied as absorbed, and a new incident bundle history begun. Otherwise, reflection must occur.

Angles of Reflection From Cone Surface

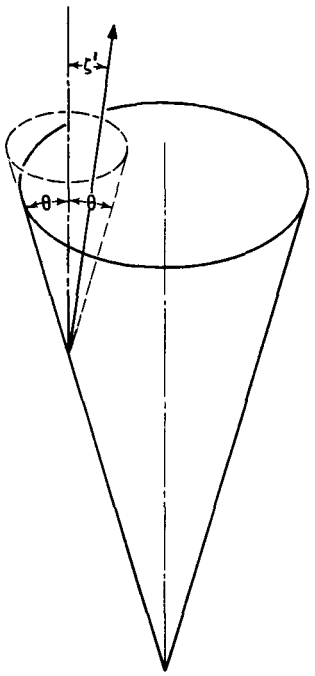

Figure 5. - Reflection from cone mouth.

The angles of reflection from a diffuse wall are determined by the relations

$$\psi = 2\pi R_{\psi} \tag{19}$$

$$\cos \eta = \sqrt{R_{\eta}} \tag{20}$$

as derived in reference 7 for reflection from a diffuse surface.

Determination of Bundle Destination

If the bundle is reflected from the position μ, φ on the cone surface at angles η' and ψ', the next step is to determine its destination. The angle to the cone axis ζ' at which the bundle is reflected gives one convenient check (fig. 5), for the bundle must leave the cone mouth if

$$\cos \zeta' < \cos \theta \tag{21a}$$

where the equation for $\cos \zeta'$ is found by resolving ℓ into its components along X', Y', and Z', projecting the components along Z, and then equating the sum of these components with the direct projection of ℓ along Z. This procedure gives

$$\cos \zeta' = \sin \theta \cos \eta' + \cos \theta \sin \eta' \cos \psi' \tag{21b}$$

If $\zeta' \geq \theta$, the bundle may or may not leave the mouth, however, and a further check is needed.

If the bundle may hit the cone wall, this fact can be determined by finding the point (μ', φ') on the wall or its extension where it will strike. The determination is discussed in the next section. If

$$\mu' \leq 1 \tag{22}$$

the bundle will strike the cone surface.

Determination of Point of Intersection With Cone Surface

The value of the point of intersection (μ', φ') must be determined in terms of the last point of reflection (μ, φ) and the angles of reflection from that point (η', ψ').

In appendix A, it is shown that

$$\cos(\angle r, r') = \cos^2\theta + \sin^2\theta \cos(\varphi' - \varphi) \tag{23}$$

When equation (23) is substituted into the law of cosines for certain imaginary triangles within the cone, it is shown further in appendix A that two independent equations are obtained:

$$\ell^2 = r^2 + r'^2 - 2rr'\left[\cos^2\theta + \sin^2\theta \cos(\varphi' - \varphi)\right] \tag{24}$$

$$\ell^2 \sin^2\zeta' = \sin^2\theta\left[r'^2 + r^2 - 2rr' \cos(\varphi' - \varphi)\right] \tag{25}$$

A third relation can also be found:

$$r'^2 = r^2 + \ell^2 + 2r\ell \sin\eta' \cos\psi' \tag{26}$$

When equation (21b) and equations (24) to (26) are used, φ' is obtained as

$$\varphi' = \varphi + \cos^{-1} \frac{r - r' \cos^2\theta \pm \dfrac{(r' - r)\sin\eta' \cos\psi' \cos\theta}{\cos\zeta'}}{r' \sin^2\theta} \tag{27}$$

with choice of the top sign being dictated by examination of the special case of $\varphi' - \varphi = \pi$, $\theta = 30^\circ$, $\eta' = 2\theta$, and $\zeta' = (\pi/2) + \theta$.

Considerable algebraic manipulation gives

$$r' = r \frac{1 - C \pm (B^2 - C)}{(1 - B^2)} \tag{28}$$

where

$$B = \frac{\cos\zeta'}{\cos\theta}$$

and

$$C = \frac{\cos \zeta' \sin \eta' \cos \psi'}{\cos \theta}$$

Examination of the special case of reflection in a direction normal to μ, φ shows that the plus sign must be chosen in equation (28).

The value of μ' is of course found directly from r' by the relation

$$\mu' = r' \sin \theta \tag{29}$$

and substitution of the value of r' into equation (27) gives φ'. If μ', φ' is indeed on the cone surface, it is again determined whether absorption will occur. If the bundle is not absorbed, new angles of reflection are determined, and this process is continued until the bundle is either absorbed at the cone surface or reflected from the mouth of the cone.

If the bundle is reflected from the mouth of the cone, the angles of reflection with respect to the cone axis (γ' and ζ') must be determined (fig. 1, p. 4).

Determination of Angles of Reflection From Cone

The angle of reflection ζ' can be computed by the equality given in equation (21). The angle γ' can be computed from the value of φ' at the last point of reflection (μ', φ') and the angles of reflection from that point (η', ψ'). This relation is derived in appendix A as

$$\gamma' = \varphi' - \cos^{-1} \frac{\cos \zeta' \sin \theta - \cos \eta'}{\sin \zeta' \cos \theta} \tag{30}$$

Care is taken in using this relation to avoid the problems inherent in allowing the digital computer to choose the principal values in evaluating trigonometric functions.

The angles at which the bundle leaves are then examined to find which increment $(\Delta\gamma', \Delta\zeta')$ it passes through on the surface of the imaginary hemisphere over the cone, and is tallied in that increment. After a sufficient number of bundle histories are followed, the values of the directional properties are computed.

The computer program is written in the Fortran IV language and run on the IBM 7094 digital computer. The program is relatively straightforward, as can be deduced from the flow chart (fig. 6, p. 12).

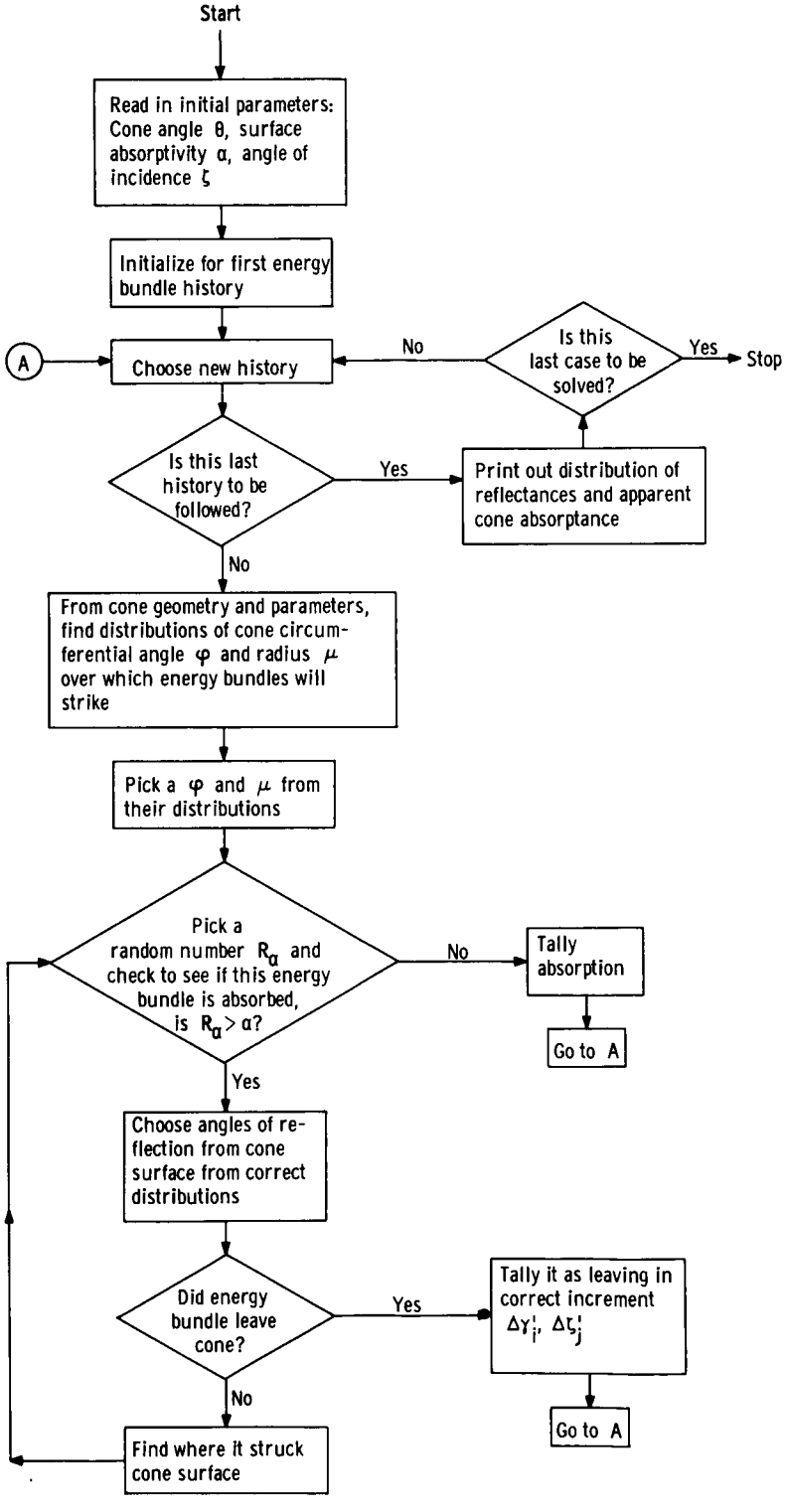

Figure 6. - Computer flow chart.

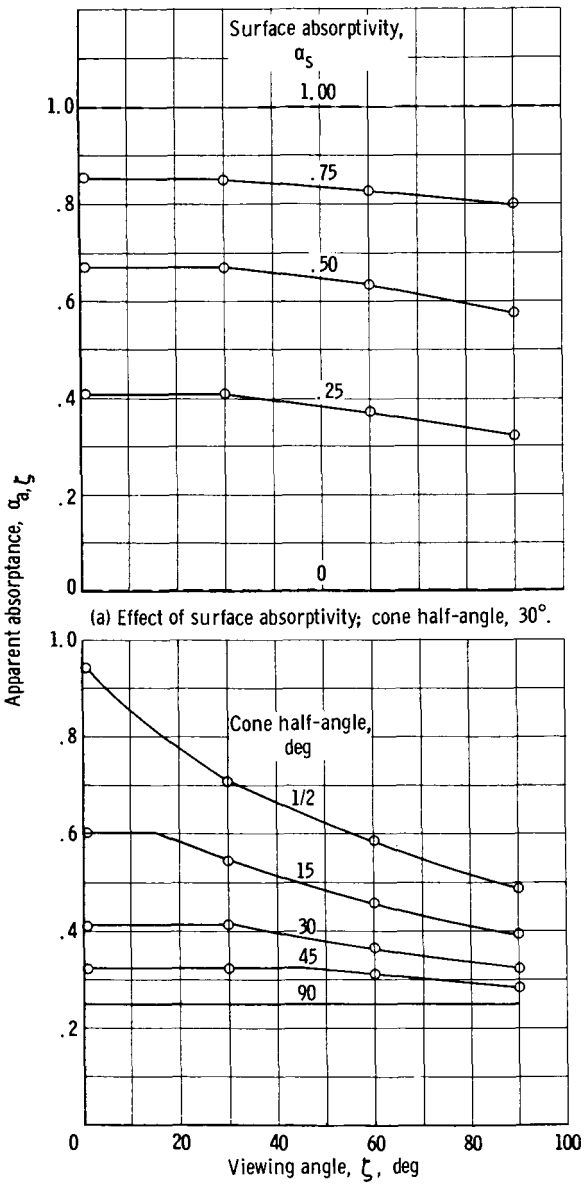

(a) Effect of surface absorptivity; cone half-angle, 30°.

(b) Effect of cone half-angle; cone surface absorptivity, 0.25.

Figure 7. - Apparent absorptance.

Running time is primarily a function of the number of histories followed and the cone half-angle θ. The half-angle affected the number of internal reflections. For θ of $1/2^{\circ}$ and any given angle of incidence and surface absorptivity, the running time for 50 000 histories was about 9 minutes. For the same conditions but with θ of 89.9°, running time was 3.5 minutes. Surface absorptivity also has some effect; for an almost black surface, most bundles are absorbed on the first encounter with a wall, and few reflections need be followed.

DISCUSSION OF RESULTS

The apparent directional absorptance of a conical cavity is shown in figure 7. As has been derived in reference 4, the directional absorptance is equal to the directional emittance for any isothermal cavity. This is true for monochromatic radiation or, for a cavity with a gray surface, for the total directional absorptance.

The apparent absorptance for a cone of any angle is always greater than the cavity surface absorptivity because of multiple reflections within the cone. The maximum apparent absorptances $\alpha_{a,\zeta}$ occur for the smallest angles of incident radiation ζ. For large angles of incidence, $\alpha_{a,\zeta}$ diminishes because the fraction of incident energy undergoing multiple reflections is reduced. Only that part of the cavity wall near the lip is illuminated by the incoming radiation.

Figure 8 depicts the directional reflectance of a cone with a 15° half-angle for radiation incident at 60° to the cone axis.

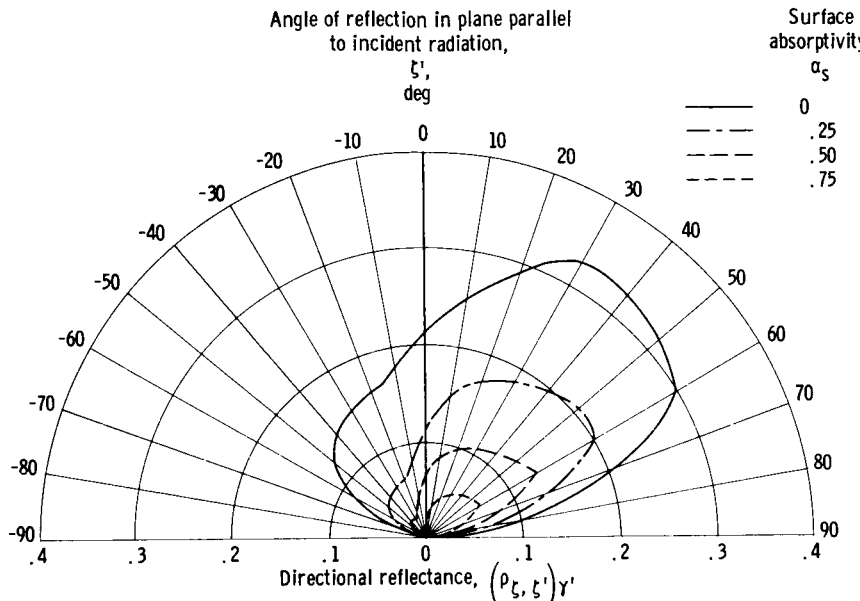

Figure 8. - Directional reflectance of conical cavity. Angle of incidence, 60°; cone half-angle, 15°.

The results in figure 8 are shown only in the plane containing the cone axis and the direction of incident radiation, and the effect of surface absorptivity is demonstrated.

In figure 9, the directional reflectance of perfectly reflecting cones with various cone half-angles between $1/2^{\circ}$ and 89.9° is presented for four angles of incident radiation. Results are given in two planes, each perpendicular to the base of the conical cavity and containing the cone axis. One plane is parallel to the direction of incident radiation, and the other is perpendicular to that plane. The most striking result is the presence of strong reflections occurring in the direction of the incident radiation, especially at the smaller cone angles. A secondary peak occurs opposite the strong reflection because of the internal reflections within the cone. The secondary peaks should decrease rapidly in magnitude with increasing surface absorptivity. As the cone angle is increased, the results approach the curve for a diffuse flat plate as expected.

Figure 10 (p. 17) presents the circumferential variation of reflectivity for various combinations of parameters, again showing the generally preferred reflection to the direction of incident radiation.

Statistical variations in the Monte Carlo results are pictured in figure 11 (p. 18) for a representative case to indicate the probable accuracy of the results. Because the angular increments become quite small near the normal to the cavity base, the number of Monte Carlo energy bundles passing through these increments is small. The small number leads to larger expected deviations near the normal.

The interesting parallel between the reflectivity results of conical cavities and those for the surface of the Moon is noted in figure 12 (p. 18). The observed lunar values given in reference 2 are compared to the normalized reflectivity results computed by the

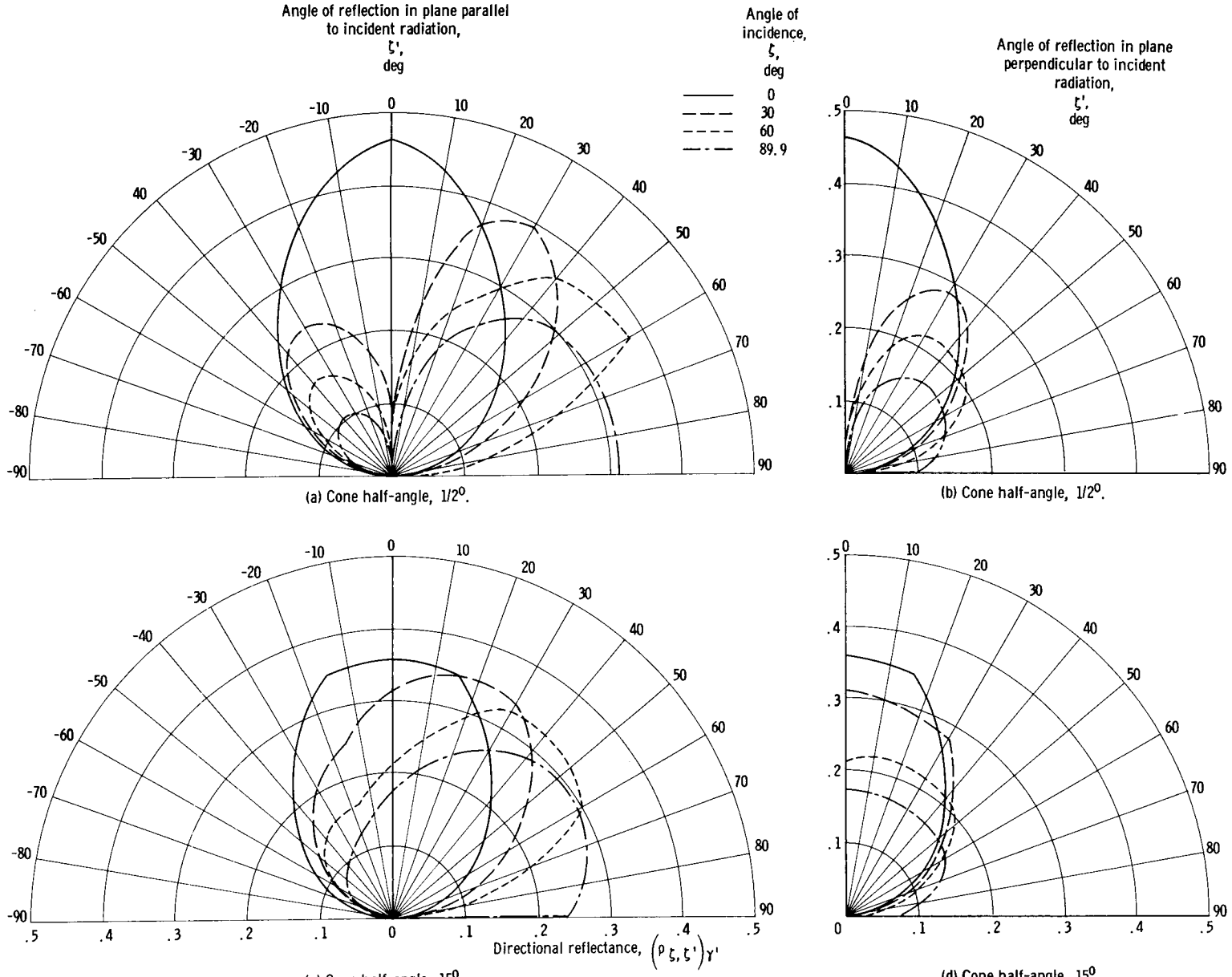

(a) Cone half-angle, 1/2°.

(b) Cone half-angle, 1/2°.

(c) Cone half-angle, 15°.

(d) Cone half-angle, 15°.

Figure 9. - Directional reflectance of conical cavity. Cone surface absorptivity, 0.

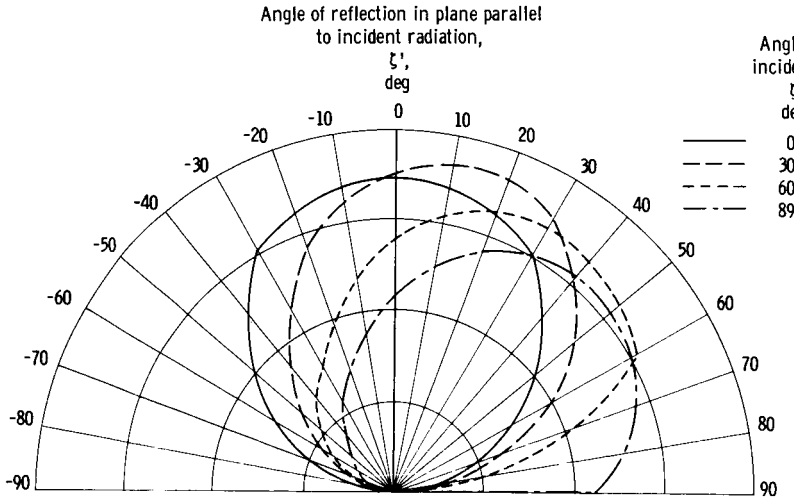

(e) Cone half-angle, 30^{0}.

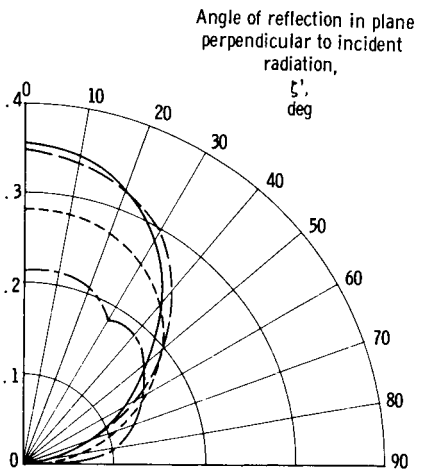

(f) Cone half-angle, 30^{0}.

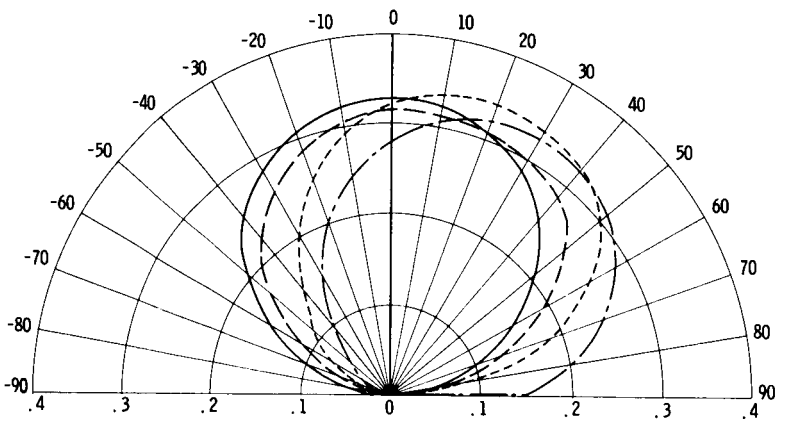

(g) Cone half-angle, 45^{0}.

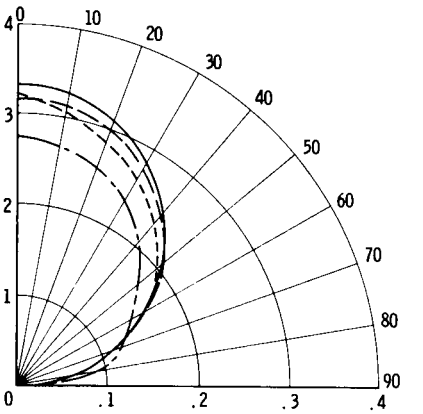

(h) Cone half-angle, 45^{0}.

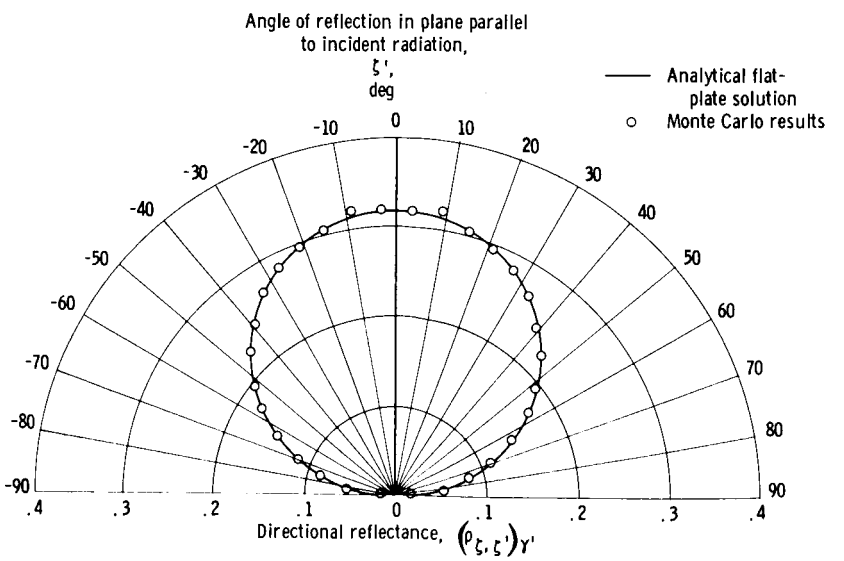

(i) Cone half-angle, 89.9^{0}; comparison of Monte Carlo and analytical solutions.

Figure 9. - Concluded.

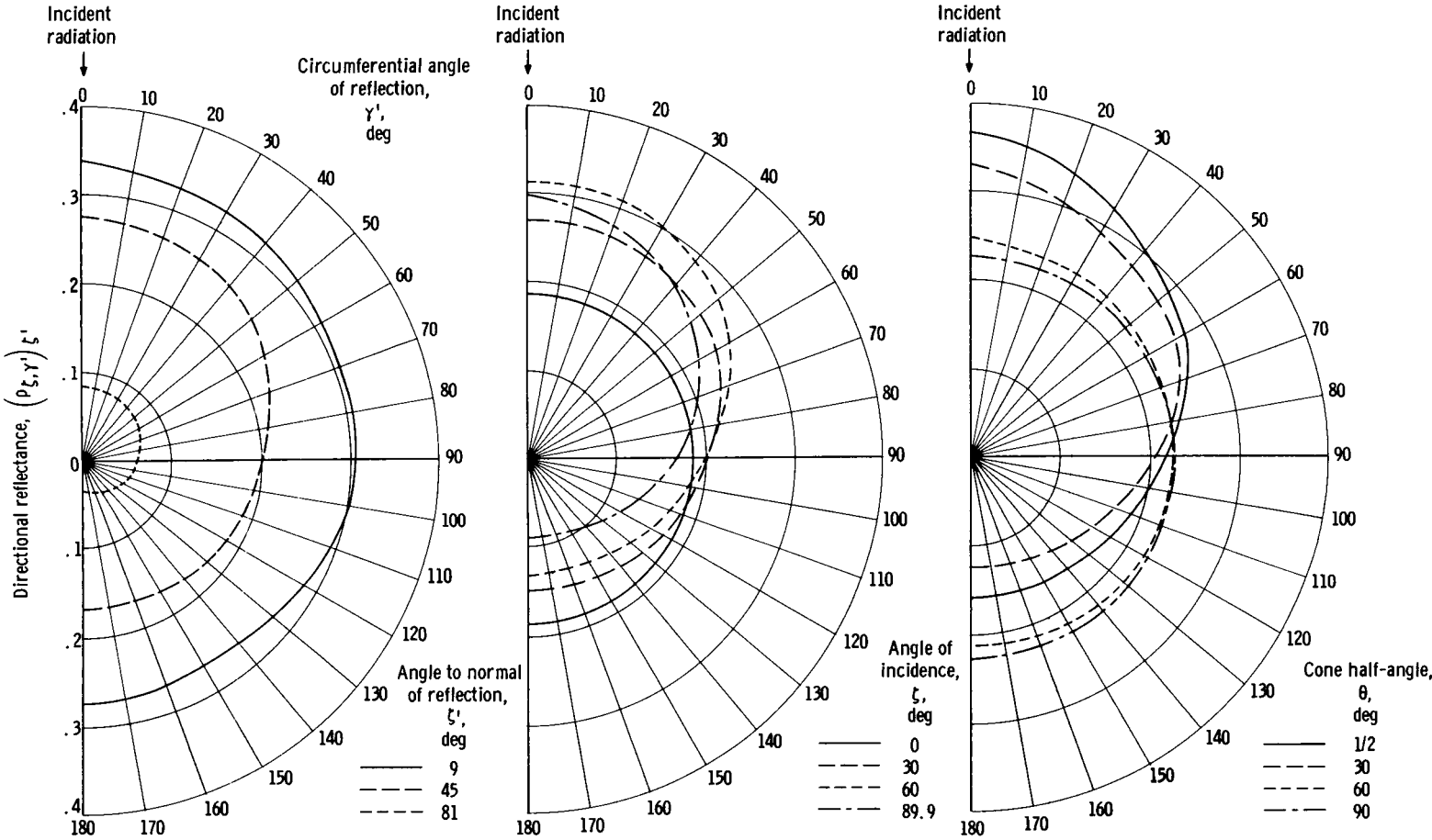

(a) Cone half-angle, 15^0; angle of incidence, 30^0.

(b) Cone half-angle, 15^0; angle to normal of reflection, 45^0.

(c) Angle of incidence, 60^0; angle to normal of reflection, 45^0.

Figure 10. - Circumferential distribution of reflectance. Cone surface absorptivity, 0.

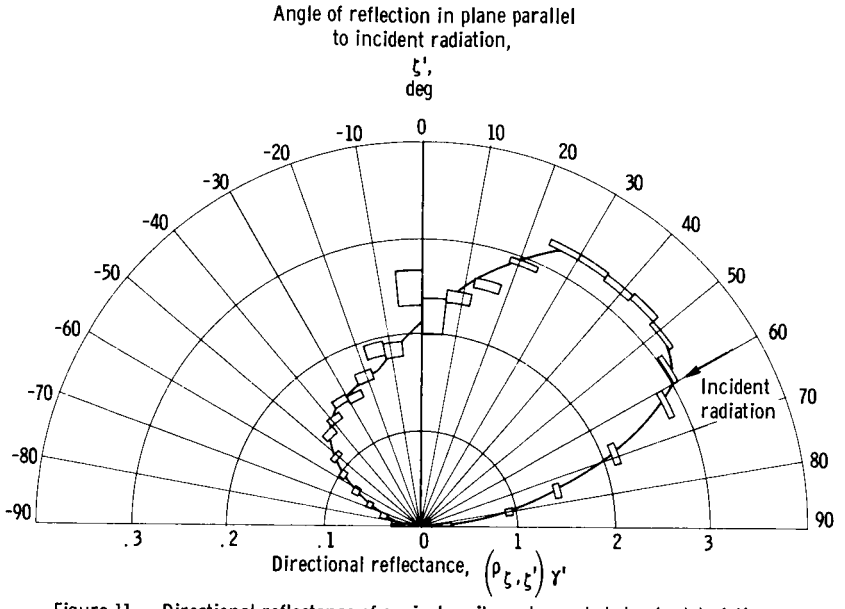

Figure 11. - Directional reflectance of conical cavity and expected standard deviation. Cone absorptivity, 0; cone half-angle, 15^0.

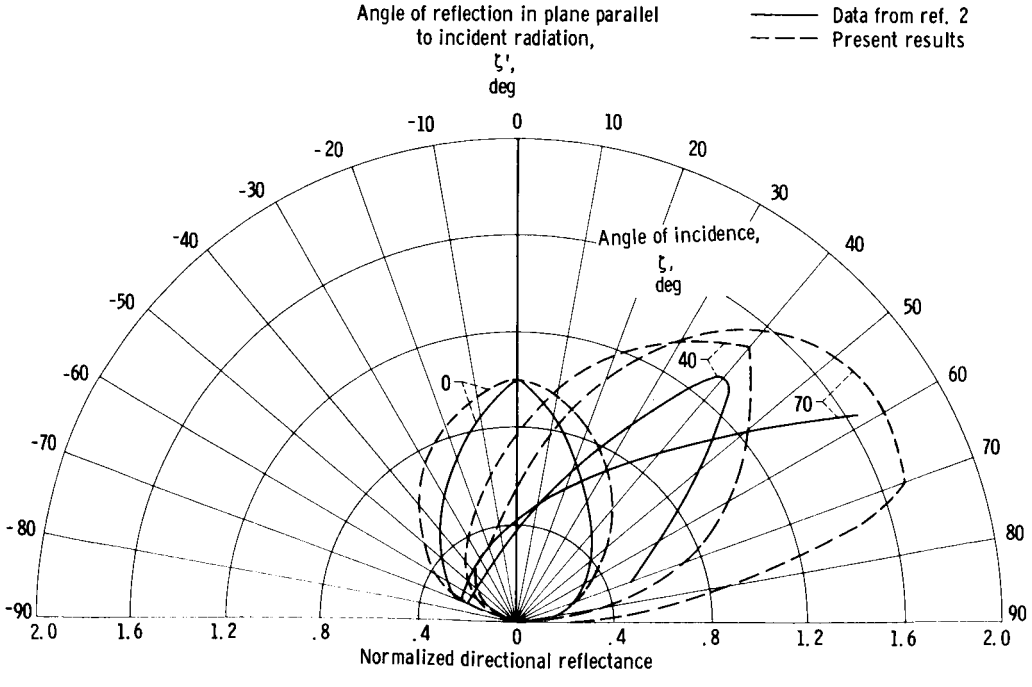

Figure 12. - Normalized directional reflectance of lunar surface from reference 2 compared to conical cavity results. Cone half-angle, 15^0; surface absorptivity, 0.5.

method of this report for a conical cavity with a half-angle of 15° and a surface absorptivity of 0.5. The similarity of these results may indicate some facts about the fine structure of the lunar surface. First, small surfaces near the normal might be expected to exist because of the relatively small cone angle which provides the similarity. Second, the lunar craters of small size which were observed by photographs from the Ranger lunar probes probably do not contribute greatly to these reflectivity effects. This is because the crater half-angles are much greater than 15°, more often approaching 60°. The reflectivity effects must therefore be based on much smaller structure.

CONCLUSIONS

The apparent absorptance and directional reflectance of conical cavities with diffusely reflecting internal surfaces are determined by a Monte Carlo procedure. The Monte Carlo technique is found to be a useful tool for solving problems of this type and appears to offer promise, especially for complex geometries.

Analytical results indicate that a strong preferential reflection in the direction of the incident beam of radiation is present and is most apparent at small cone angles. Because the only limitation on the size of cavities causing these effects is that they be large compared to the wavelength of incident radiation, it is possible that surface microstructure could strongly affect the reflectance of engineering surfaces. Measurements made on polished laboratory samples will probably not predict the directional behavior of less highly finished surfaces.

Lewis Research Center,
National Aeronautics and Space Administration,
Cleveland, Ohio, April 14, 1965.

APPENDIX A

DERIVATION OF BUNDLE PATH EQUATIONS

Relations Between Incident Angle

In figure 13, the interrelations between angles for an incident bundle are shown. To derive an expression for the angle η in terms of the angles ζ, θ, and φ, the length $\mathcal{O} - \mathcal{B}'$ can be divided as

$$(\mathcal{O} - \mathcal{B}') = (\mathcal{O} - \mathcal{B}) + (\mathcal{B} - \mathcal{B}') \tag{A1}$$

Then

$$(\mathcal{O} - \mathcal{B}') = (\mathcal{O} - \mathcal{I})\cos \eta \tag{A2}$$

and

$$(\mathcal{O} - \mathcal{B}) = \frac{(\mathcal{O} - \mathcal{C})}{\cos \theta} = \frac{(\mathcal{O} - \mathcal{A})}{\cos \theta} = \frac{(\mathcal{O} - \mathcal{I})\sin \zeta \cos \varphi}{\cos \theta} \tag{A3}$$

Also,

$$(\mathcal{B} - \mathcal{B}') = (\mathcal{A} - \mathcal{B})\sin \theta = [(\mathcal{A} - \mathcal{C}) - (\mathcal{B} - \mathcal{C})]\sin \theta \tag{A4}$$

where

$$(\mathcal{A} - \mathcal{C}) = (\mathcal{O} - \mathcal{I})\cos \zeta \tag{A5}$$

and

$$(\mathcal{B} - \mathcal{C}) = (\mathcal{O} - \mathcal{C})\tan \theta = (\mathcal{O} - \mathcal{I})\sin \zeta \cos \varphi \tan \theta \tag{A6}$$

Substituting (A2) to (A6) into (A1) gives

$$\cos \eta = \frac{\sin \zeta \cos \varphi}{\cos \theta} + \cos \zeta \sin \theta - \sin \zeta \cos \varphi \sin \theta \tan \theta = \cos \zeta \sin \theta + \sin \zeta \cos \theta \cos \varphi \tag{A7}$$

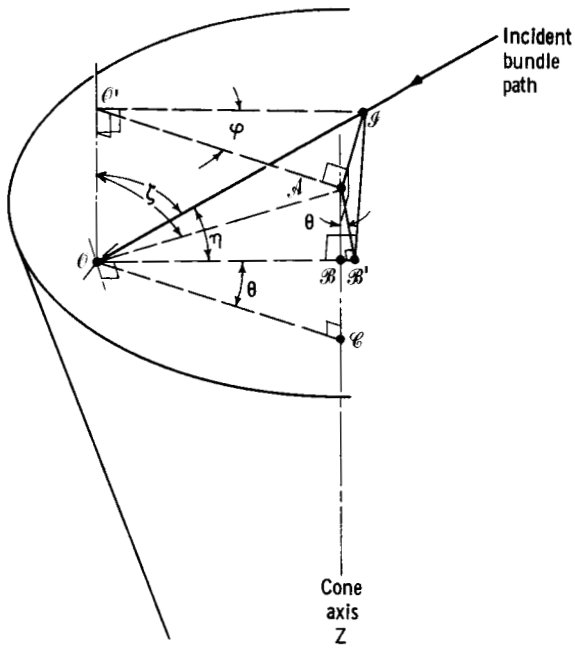

Figure 13. - Relations between angles for incident bundle.

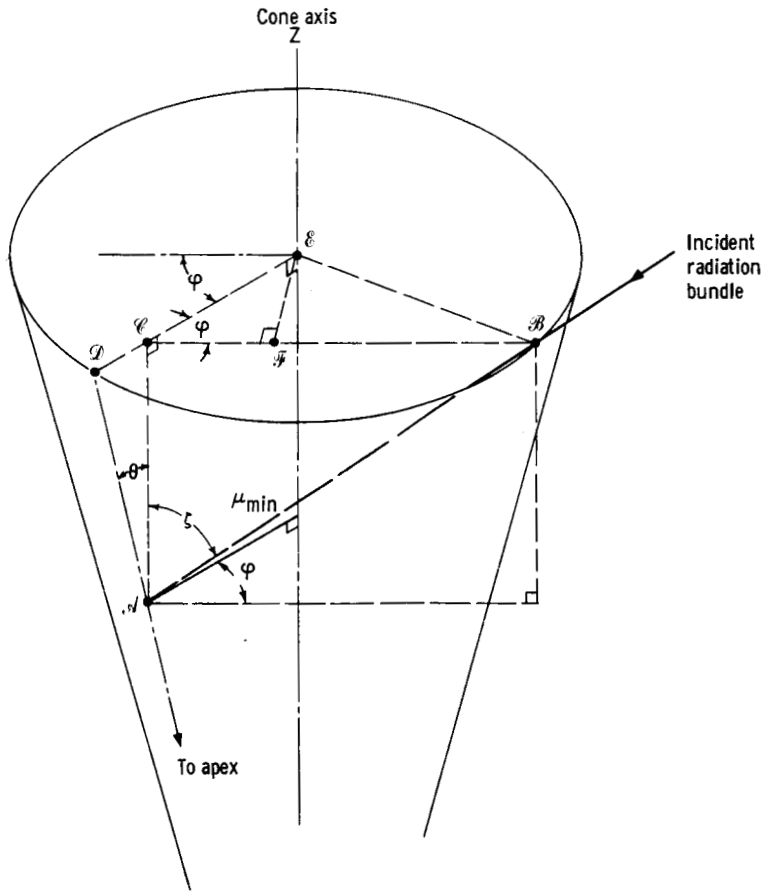

Figure 14. - Relations for μ_{min}.

Derivation of μ_{min} Relations

The minimum point on the interior surface of the cone at which a bundle may strike for a given value of the angle φ can be derived by referring to figure 14. The line $(\mathscr{A} - \mathscr{C})$ has a length given by

$$(\mathscr{A} - \mathscr{C}) = (\mathscr{D} - \mathscr{C})\cot\theta = (1 - \mu_{min})\cot\theta \tag{A8}$$

or, alternately

$$(\mathscr{A} - \mathscr{C}) = (\mathscr{B} - \mathscr{C})\tan(90 - \zeta) \tag{A9}$$

where

$$(\mathscr{B} - \mathscr{C}) = (\mathscr{C} - \mathscr{F}) + (\mathscr{F} - \mathscr{B}) = \mu_{min}\cos\varphi + (1 - \mu_{min}^2 \sin^2\varphi)^{1/2} \tag{A10}$$

Substituting (A10) into (A9), and equating the result to (A8) gives

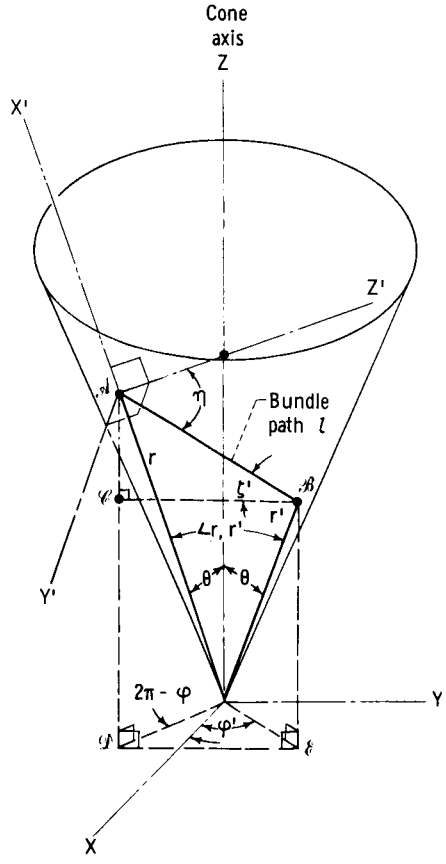

Figure 15. - Derivation of bundle path relations.

$$(1 - \mu_{min})\cot\theta = \tan(90 - \zeta) \times \left[\mu_{min}\cos\varphi + (1 - \mu_{min}^2 \sin^2\varphi)^{1/2}\right] \tag{A11}$$

Derivation of Bundle Path Relations

The bundle path relations may be found from figure 15 by writing the law of cosines for triangles $(\mathscr{A}\mathscr{O}\mathscr{B})$, $(\mathscr{D}\mathscr{O}\mathscr{E})$, and $(\mathscr{A}\mathscr{B}\mathscr{C})$, to give, respectively

$$\ell^2 = r^2 + r'^2 - 2rr'\cos(\angle r, r') \tag{A12}$$

$$(\mathscr{D} - \mathscr{E})^2 = \ell^2 \sin^2\zeta' = r^2 \sin^2\theta + r'^2 \sin^2\theta - 2rr' \sin^2\theta \cos(\varphi' - \varphi) \tag{A13}$$

$$\ell^2 = (\mathscr{D} - \mathscr{E})^2 + (r\cos\theta - r'\cos\theta)^2 \tag{A14}$$

Combining to eliminate ℓ^2 and $(\mathscr{D} - \mathscr{E})$ gives

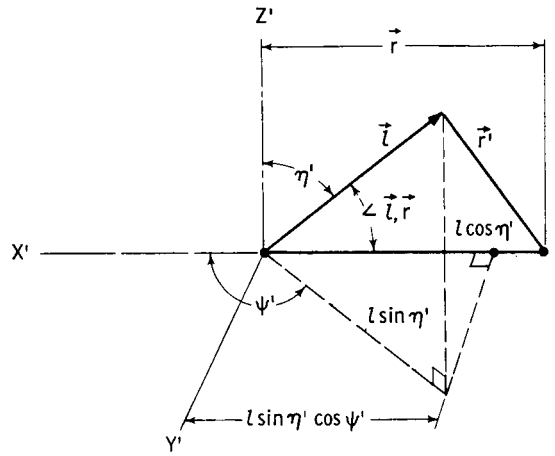

Figure 16. - Auxiliary coordinates along cone wall.

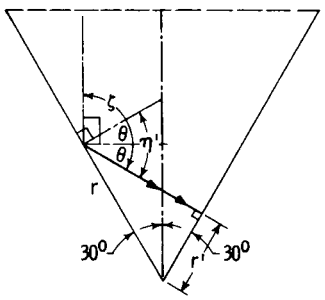

Figure 17. - Choice of sign in equation (27).

$$\cos(\angle r, r') = \cos^2\theta + \sin^2\theta \cos(\varphi' - \varphi) \tag{A15}$$

Also, using the coordinates shown in figure 16, the law of cosines gives

$$r'^2 = r^2 + \ell^2 - 2r\ell \cos(\angle \ell, r) \tag{A16}$$

but

$$\cos(\angle \ell, r) = -\frac{\ell \sin\eta' \cos\psi'}{\ell} \tag{A17}$$

and substituting (A17) into (A16) gives

$$r'^2 = r^2 + \ell^2 + 2r\ell \sin\eta' \cos\psi' \tag{A18}$$

Correct Choice of Sign for Equation (27)

Figure 17 shows the special case of cone angle $\theta = 30^o$, incident angle $\zeta = \pi/2 + \theta = 120^o$, and the reflected bundle passing through the cone axis. It follows that $\eta' = 2\theta = 60^o$, $\psi' = \pi$, and $(\varphi' - \varphi) = \pi$. Also, the point of intersection on the cone wall, r', is related to r by

$$r' = r \sin\theta = \frac{r}{2} \tag{A19}$$

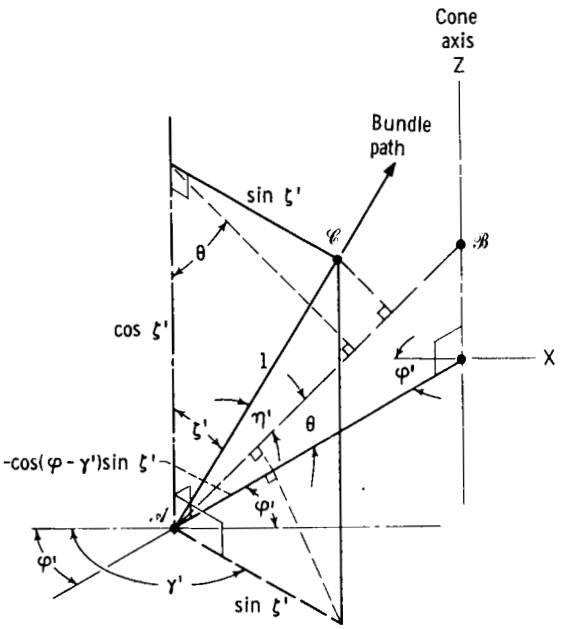

Figure 18. - Determination of bundle exit direction.

Substituting into equation (27) gives

$$\cos(\varphi' - \varphi) = -1 = \frac{r - r' \cos^2\theta \pm \dfrac{(r' - r)\sin\eta' \cos\psi' \cos\theta}{\cos\zeta'}}{r' \sin^2\theta} = \frac{2r' - \dfrac{3r'}{4} \pm \left[\dfrac{(-r')\dfrac{\sqrt{3}}{2}\dfrac{\sqrt{3}}{2}(-1)}{\left(-\dfrac{1}{2}\right)}\right]}{\dfrac{1}{4}r'} \tag{A20}$$

or

$$-\frac{1}{4} = \frac{5}{4} \pm \left(\frac{-6}{4}\right) \tag{A21}$$

from which it follows that the plus sign must be chosen.

Determination of Bundle Exit Direction

From figure 18, it can be seen that the direct projection of the length ($\mathscr{A}$-$\mathscr{C}$) = 1

directly onto ($\mathscr{A}$ - $\mathscr{B}$) is simply cos η. Projection of ($\mathscr{A}$ - $\mathscr{C}$) onto ($\mathscr{A}$ - $\mathscr{B}$) by components gives

$$(\mathscr{A} - \mathscr{C})\cos\eta = (\mathscr{A} - \mathscr{C})\left[\cos\zeta' \sin\theta + (-\cos(\varphi' - \gamma')\sin\zeta' \cos\theta)\right] \tag{A22}$$

or

$$\gamma' = \varphi' - \cos^{-1}\frac{\cos\zeta' \sin\theta - \cos\eta}{\sin\zeta' \cos\theta} \tag{A23}$$

APPENDIX B

SOLUTION TECHNIQUE FOR TRANSCENDENTAL EQUATION

The transcendental equation in φ (eq. (27)) was solved by using a modified Newton-Raphson technique. The standard Newton-Raphson expression is

$$\varphi = \varphi_0 - \frac{f(\varphi_0)}{f'(\varphi_0)} \tag{B1}$$

where φ_0 is the value of φ from the previous iteration. When a third-order term is desired, the form is

$$\varphi - \varphi_0 = -\frac{f(\varphi_0)}{f'(\varphi_0)}(1 + \delta) \tag{B2}$$

The Taylor series expansion of φ when $f(\varphi) = 0$ is

$$0 = f(\varphi_0) + f'(\varphi_0)(\varphi - \varphi_0) + \frac{f''(\varphi_0)}{2}(\varphi - \varphi_0)^2 + \cdots \tag{B3}$$

Substituting equation (B2) into (B3) gives

$$0 = f(\varphi_0) + f'(\varphi_0)\frac{-f(\varphi_0)}{f'(\varphi_0)}(1 + \delta) + \frac{f''(\varphi_0)}{2}\left[\frac{f(\varphi_0)}{f'(\varphi_0)}\right]^2(1 + \delta)^2 + \cdots \tag{B4}$$

For $|\delta| \ll 1$, δ^2 and higher order terms may be neglected, and thus

$$\delta = \frac{f''(\varphi_0)\left[f(\varphi_0)\right]^2}{2\left\{f(\varphi_0)\left[f'(\varphi_0)\right]^2 - f''(\varphi_0)\left[f(\varphi_0)\right]^2\right\}} \tag{B5}$$

Substituting into equation (B2) results in

$$\varphi = \varphi_0 - \frac{f(\varphi_0)}{f'(\varphi_0)} \frac{2\left[f'(\varphi_0)\right]^2 - f''(\varphi_0)f(\varphi_0)}{2\left\{\left[f'(\varphi_0)\right]^2 - f''(\varphi_0)f(\varphi_0)\right\}} \tag{B6}$$

which is the Newton-Raphson expression modified.

For small values of f', the Newton-Raphson technique provides slow convergence. In such cases, the regula-falsi method was used. The latter technique works best for small values of f'.

In the computer program, 25 iterations were allowed to provide convergence such that the φ calculated in successive iterations differed by less than 10^{-3}. A sampling of test cases showed that, on the average, three iterations and seldom over five iterations were required for convergence when the modified Newton-Raphson technique was used. It was rarely necessary to use the auxiliary regula-falsi method for determining φ.

REFERENCES

1. Birkebak, R. C.; Sparrow, E. M.; Eckert, E. R. G.; and Ramsey, J. W.: Effect of Surface Roughness on the Total Hemispherical and Specular Reflectance of Metallic Surfaces. J. Heat Transfer (Trans. ASME), ser. C, vol. 86, no. 2, May 1964, pp. 193-199.

2. Orlova, N. S.: Photometric Relief of the Lunar Surface. Astron. Zh. (Moscow), vol. 33, no. 1, Jan.-Feb. 1956, pp. 93-100.

3. Brandenberg, W. M.; and Clausen, O. W.: The Directional, Spectral Emittance of Surfaces Between 200 and 600° C. Rept. No. ERR-AN-342 (GD/A 63-1037), General Dynamics/Astronautics, Oct. 1963.

4. Howell, John R.; and Perlmutter, Morris: Directional Behavior of Emitted and Reflected Energy from a Specular, Gray, Asymmetric Groove. NASA TN D-1874, 1963.

5. Sparrow, E. M.; and Jonsson, V. K.: Radiant Emission Characteristics of Diffuse Conical Cavities. J. Opt. Soc. Am., vol. 53, no. 7, July 1963, pp. 816-821.

6. Hildebrand, F. B.: Introduction to Numerical Analysis. McGraw-Hill Book Co., Inc., 1956, pp. 446-447.

7. Howell, J. R.; and Perlmutter, M.: Monte Carlo Solution of Thermal Transfer Through Radiant Media Between Gray Walls. J. Heat Transfer (Trans. ASME), ser. C, vol. 86, no. 1, Feb. 1964, pp. 116-122.